Theory of higher harmonics imaging in tapping-mode atomic force microscopy*

Li Yuan(李 渊), Qian Jian-Qiang(钱建强)†, and Li Ying-Zi(李英姿)

Department of Applied Physics, Beihang University, Beijing 100191, *China*

(Received 14 September 2009; revised manuscript received 28 October 2009)

The periodic impact force induced by tip-sample contact in a tapping mode atomic force microscope (AFM) gives rise to the non-harmonic response of a micro-cantilever. These non-harmonic signals contain the full characteristics of tip-sample interaction. A complete theoretical model describing the dynamical behaviour of tip–sample system was developed in this paper. An analytic formula was introduced to describe the relationship between time-varying tip–sample impact force and tip motion. The theoretical analysis and numerical results both show that the time-varying tip–sample impact force can be reconstructed by recording tip motion. This allows for the reconstruction of the characteristics of the tip–sample force, like contact time and maximum contact force. It can also explain the ability of AFM higher harmonics imaging in mapping stiffness and surface energy variations.

Keywords: tapping mode atomic force microscopy, higher harmonics imaging
PACC: 0779, 6116P, 6240

1. Introduction

Since its invention in 1986, the atomic force microscope (AFM)[1] has been widely used for nanometer-scale characterization and modification of surfaces in air and liquid environments.[2,3] Amplitude modulation atomic force microscope, also known as tapping mode AFM,[4] has been found to be more gentle compared to the contact mode AFM, since the lateral force acting on the sample are dramatically reduced. High resolution image of DNA, antibodies, polymers and silicon have been obtained as well as true atomic resolution images of inorganic surface.[5−7]

Several related techniques have been developed aiming at the interactions and the underlying material properties. The phase shift existing between the excitation and the cantilever's response has been proposed and applied to generate compositional maps of heterogeneous surfaces.[8−10] However, interpretation of this phase imaging data is still controversially discussed in the literatures.[11−14]

The need to improve compositional contrast has stimulated the development of methods based on the detection and excitation[15,16] of higher harmonics or modes. Garcia *et al.* firstly proposed a method for mapping the composition of a surface by simultaneously exciting the first two modes of the cantilever.[17,18] Theoretical simulation and experiment results both show that the multifreqency AFM could result in higher force sensitivity and compositional contrast.[19−21]

The tip periodically tapping on the sample surface gives rise to a periodic pulse like tip–sample force, which generates high frequency vibration also known as higher harmonics.[22,23] Stark and Heckel have calculated the contribution of the higher harmonics to the tip deflection under the periodic external repulsive force, and proposed that higher harmonics signal contains the information on the elastic properties of the specimen.[24] Legleiler *et al.* have used higher harmonics to extract the time-resolved force interaction in fluids.[25]

These dynamic microcopies are based on the fact that the entire interaction is encoded into the cantilever motion. But these methods can only partly reflect the mechanical properties of the sample surface, for none of these utilizes the full information of the tip motion.

In this paper, we study the tip motion of a rectangular cantilever tapping on the sample surface, and a theory is put forward to resolve the time-dependent tip–sample impact force by recording and analysing the tip motion.

*Project supported by the National High-Tech Research and Development Program of China (Grant No. 2007AA12Z128).
†Corresponding author. E-mail: qianjq@buaa.edu.cn
© 2010 Chinese Physical Society and IOP Publishing Ltd

2. Model

The one-dimensional Euler–Bernoulli equation governs the dynamics of a rectangular cantilever. For the model calculations here, the mass of the tip is neglected, thus the equation of motion for transversal cantilever vibrations is[24]

$$\begin{aligned} &EI\frac{\partial^4}{\partial x^4}\left(w(x,t)+a_1\frac{\partial w(x,t)}{\partial t}\right)\\ &+\rho bh\frac{\partial^2 w(x,t)}{\partial t^2}+a_0\rho\frac{\partial w(x,t)}{\partial t}\\ &=\delta(x-L)\left(f_{\rm ext}(t)+F_{\rm ts}(d,\dot{d})\right). \end{aligned} \tag{1}$$

E is the cantilever's Young's modulus, I is the moment of inertia. Damping is modeled by two parameters a_0 and a_1, a_0 is the hydrodynamic damping coefficient, and a_1 is the internal damping coefficient; ρ is the mass density, b, h, and L are, respectively, the width, height, and length of the cantilever; $w(x,t)$ is the time-dependent vertical displacement of the differential beam's element placed at the x position. $F_{\rm ext}(t)$ is the excitation force; while the tip–sample interaction is represented by $F_{\rm ts}(d,\dot{d})$ with $d=z_c+w(L,\,t)$ being the instantaneous tip–sample separation.

The cantilever is clamped at $x=0$ while it is free at $x=L$. Hence, the following boundary conditions apply[26]

$$\begin{aligned} &w(0,t)=\left.\frac{\partial w(x,t)}{\partial x}\right|_{x=0}=0,\\ &\left.\frac{\partial^2 w(x,t)}{\partial x^2}\right|_{x=L}=\left.\frac{\partial^3 w(x,t)}{\partial x^3}\right|_{x=L}=0. \end{aligned} \tag{2}$$

The above boundary conditions introduce a discrete number of solutions to Eq. (1). Then the vertical displacement can be expanded into a series of eigenmodes,

$$w(x,t)=\sum\nolimits_{n=1}^{\infty}\varphi_n(x)Y_n(t), \tag{3}$$

where $\varphi_n(x)$ can be defined as

$$\begin{aligned} \varphi_n(x)=&\cos(\kappa_n x)-\cosh(\kappa_n x)\\ &-\frac{\cos(\kappa_n L)+\cosh(\kappa_n L)}{\sin(\kappa_n L)+\sinh(\kappa_n L)}\\ &\times(\sin(\kappa_n x)-\sinh(\kappa_n x)), \end{aligned} \tag{4}$$

with κ_n being the nth positive real root of the equation

$$\cos(\kappa_n L)\cosh(\kappa_n L)+1=0. \tag{5}$$

And we have

$$\int_0^L\varphi_n(x)\varphi_m(x){\rm d}x=L\delta_{n,m}, \tag{6}$$

$$\varphi_n(0)=0, \tag{7}$$

$$\varphi(L)=2(-1)^n. \tag{8}$$

Equation (1) then can be transformed into a set of decoupled ordinary differential equations

$$\begin{aligned} &\ddot{Y}_i(t)+2\gamma_i\omega_i\dot{Y}_i(t)+\omega_i^2 Y_i(t)=\frac{F_i(t,d,\dot{d})}{M_i},\\ &i=1,2,3,\ldots. \end{aligned} \tag{9}$$

The generalised mass M_i, generalised force $F_i(t,d,\dot{d})$ and damping parameter γ_i can be expressed as

$$M_i=\int_0^L\rho A\varphi_i(x)^2{\rm d}x=\rho AL=m, \tag{10}$$

$$\begin{aligned} F_i(t,d,\dot{d})=&\int_{x=0}^{L}\delta(x-L)(f_{\rm ext}(t)\\ &+F_{\rm ts}(d,\dot{d}))\varphi_i(x){\rm d}x\\ =&(f_{\rm ext}(t)+F_{\rm ts}(d,\dot{d}))\varphi_i(L), \end{aligned} \tag{11}$$

$$\gamma_i=\frac{a_0}{2\omega_i}+\frac{a_1\omega_i}{2}. \tag{12}$$

When the cantilever oscillates in steady state, the tip–sample interaction $F_i(t,d,\dot{d})$ is a periodic function which has the same period as the excitation force, so the tip–sample interaction can be expressed as $F_i(t)$. A periodic but arbitrarily shaped generalised excitation function $F_i(t)$ with base frequency Ω can be expanded in a Fourier series as

$$F_i(t)=\sum_{k=-\infty}^{+\infty}c_{i,k}\exp({\rm i}\,k\Omega t). \tag{13}$$

Thus, the time-dependent stationary amplitude response of the individual modes ϕ_i is given by[24]

$$\begin{aligned} Y_i(t)=&\frac{1}{K_i}\sum_{k=-\infty}^{+\infty}\frac{(1-\beta_{i,k}^2)-{\rm i}(2\gamma_i\beta_{i,k})}{(1-\beta_{i,k}^2)^2+(2\gamma_i\beta_{i,k})^2}\cdot c_{i,k}\\ &\times\exp({\rm i}\,k\Omega t), \end{aligned} \tag{14}$$

where $\beta_{i,k}=k\Omega/\omega_i$ is the frequency ratio between driving force and the respective resonant frequency ω_i, and the generalised stiffness is $K_i=M_i\omega_i^2$. Introducing the complex coefficients

$$c_{i,k}^Y=\frac{1}{K_i}\cdot\frac{(1-\beta_{i,k}^2)-{\rm i}(2\gamma_i\beta_{i,k})}{(1-\beta_{i,k}^2)^2+(2\gamma_i\beta_{i,k})^2}\cdot c_{i,k}, \tag{15}$$

the steady state response to an arbitrary external force can be written as

$$w(x,t)=\sum_{i=1}^{\infty}\varphi_i(x)\sum_{k=-\infty}^{+\infty}c_{i,k}^Y\exp({\rm i}\,k\Omega t). \tag{16}$$

The movement of the end of the tip can be expressed as a Fourier series

$$w(L,t) = \sum_{k=-\infty}^{+\infty} N_k \exp(\mathrm{i}\, k\Omega t) = \sum_{i=1}^{\infty} \varphi_i(L) Y_i(t) = \sum_{i=1}^{\infty} \phi_i^2 \sum_{k=-\infty}^{+\infty} B_i^k A_k \exp(\mathrm{i}\, k\Omega t). \quad (17)$$

Exchange the order of the two summations, we can obtain

$$\sum_{k=-\infty}^{+\infty} N_k \exp(\mathrm{i}\, k\Omega t) = \sum_{i=1}^{\infty} \phi_i^2 \sum_{k=-\infty}^{+\infty} B_i^k A_k \exp(\mathrm{i}\, k\Omega t) = \sum_{k=-\infty}^{\infty} A_k \sum_{i=1}^{+\infty} \phi_i^2 B_i^k \exp(\mathrm{i}\, k\Omega t). \quad (18)$$

Thus, the relationship between the two Fourier series coefficient sets can be simply expressed as two algebraic formulas

$$N_k = A_k \sum_{i=1}^{+\infty} \phi_i^2 B_i^k, k = -\infty, \ldots, \infty; \quad (19)$$

$$A_k = \frac{N_k}{\sum_{i=1}^{\infty} \phi_i^2 B_i^k}, k = -\infty, \ldots, \infty. \quad (20)$$

Throughout this paper, Eqs. (19) and (20) are employed in order to reconstruct the characteristics of the time-dependent tip–sample force.

Actually, the forces acting on the cantilever consist of the external driving force and the tip–sample interaction force. The results directly obtain from Eq. (20) are the summation of the two forces. Only the tip–sample interaction force contains the useful information about the characteristics of the sample surface. The motion of the cantilever brought about by the external driving force can be recorded ahead and subtracted before the computation of Eq. (20).

3. Results and discussions

In the following, the detection of the higher harmonic signals is carried out within the framework of the above theory. In the numerical simulation, the conservative tip–sample interaction model is continuous but not smooth, consisting of a van der Waals force regime[2,27,28] and a contact regime based on the Derjaguin–Müller–Toporov (DMT) model[29]

$$F_{\mathrm{ts}}(d) = -\frac{AR}{6d^2}, \quad d > a_0;$$
$$F_{\mathrm{ts}}(d) = -\frac{AR}{6a_0^2} + E^*\sqrt{R}(a_0 - d)^{3/2}, \quad d \le a_0, \quad (21)$$

where d is the gap between the tip and the sample, a_0 is the intermolecular distance, which is usually introduced to avoid unphysical divergence of the tip–sample interaction force, H is the Hamaker constant, R is the radius of the tip, and $E^* = [(1-v_t^2)/E_t + (1-v_s^2)/E_s]^{-1}$, where E and ν represent respectively elastic moduli and Poisson's ratios. The non-conservative interactions can be included as an option in a simulation based on the Kelvin–Voigt viscoelastic contact damping model[30]

$$F_{\mathrm{tsnc}}(d, \dot{d}) = -\eta \dot{d} \sqrt{R(a_0 - d)}, \quad (22)$$

where η is the sample viscosity. Viscoelastic contact damping is a common feature on polymer surfaces and biological materials.[31]

We consider a cantilever that has a generalised mass $m = 2.5 \times 10^{-10}$ kg, spring constant $c = 20$ N/m, the tip radius $R = 20$ nm. The frequencies of the first five eigenmodes of the cantilever are 44.8, 280.757, 786.128, 1540.5 and 2546.55 kHz, the quality factors are 100, 300, 90.15, 49.67 and 30.59, respectively. Free oscillation amplitude (peak to peak) is 100 nm. Those values represent some of the common case for tapping-mode rectangular cantilevers. The sample parameters are Hamaker constant $A = 10^{-19}$ J, $E^* = 129$ GPa, intermolecular distance $a_0 = 0.25$ nm. The integration was performed using five coupled fourth-order Runge–Kutta algorithms.

The spectrum of the cantilever motion in tapping near the surface is show in Fig. 1. The tip–sample average separation is 60 nm (setpoint 60%). The dominant component for the cantilever dynamics is at the fundamental frequency. Due to the nonlinear tip–sample interaction the higher harmonic components of the tip motion (the sixth and the 18th harmonics) near the intrinsic vibration modes (the second and the third eigen-modes of the cantilever) are excited significantly, indicating a dependence of harmonics generation on cantilever eigen-modes. But the total contribution of the harmonic components is only about 1%. The '+' indicates the respective Fourier coefficients of tip–sample impact force. The amplitude of the impact decreases as the index of harmonics increases. The coefficients beyond 50th harmonics can be safely neglected for their relatively trivial value.

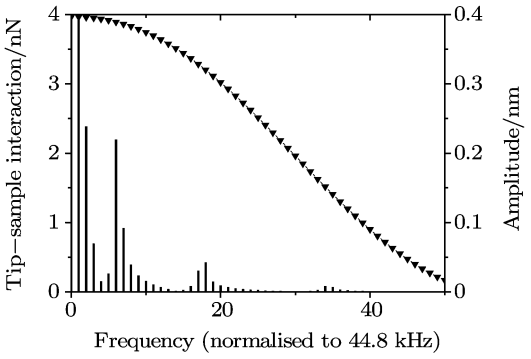


Fig. 1. The motion of the tapping cantilever in frequency domain. The amplitude of the fundamental frequency is shortened in order to fit into the figure. The down-triangle indicates the respective Fourier coefficients of the tip–sample impact.

The tip periodically tapping on the sample surface brings about a periodic pulse like force acting on both tip and sample. This pulse differs as the tip tapping on different sample surface. The time-dependent impact force curves with different sample's stiffness are shown in Fig. 2, for stiffness is a key parameter for distinguishing the compositional difference of a surface. The curves show that the maximum of the impact force increases and the tip sample contact time decreases as the sample's stiffness increases. But the impact force curves show little difference when the Young's modulus is beyond 100 GPa. Thus the tapping tip is more sensitive to the change of stiffness of softer materials. The maximum repulsive impact force is one of the parameters that can better reflect the influence of mechanical properties on tapping operation as well as the most significant parameter evaluation of sample damage.[32] The maximum attractive tip–sample force is directly related to the Hamaker constant of the sample surface (see Eq. (21)) and reflecting the surface energy variation of the sample. These two maximum values can be simply extracted from the time-dependent impact force curves.

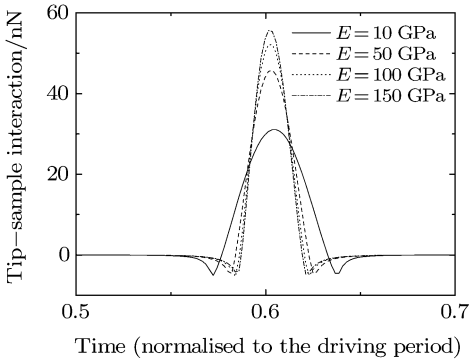


Fig. 2. The periodic tapping force for different surface elasticity determined by the numerical simulation. The average distance between the zero position of the cantilever and the sample surface is 30 nm. Sample stiffness of 10, 50, 100, and 150 GPa were used in the calculation.

In an actual scan process, the feedback control regulates the tip–sample average separation by continuously adjusting the sample's position in z direction. The control error results in a few percentage deviation of the expected tip–sample average separation, which may influence the tip–sample impact force. The tip–sample impact forces at three different tip–sample average separations were calculated and are shown in Fig. 3. As decreases the tip–sample average separation, the peak of the impact force moves ahead in time domain, but the shape of the impact force does not change. Thus, unlike the conventional method for mapping chemical composition of a surface, such as phase imaging, the surface characters acquired by the method proposed in this paper are not influenced by feedback control error.

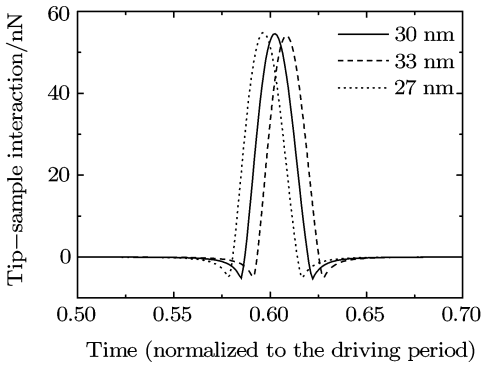


Fig. 3. The time-dependent periodic impact force at three different tip–sample average separations. Tip–sample average separations of 28.5, 30, and 31.5 nm were used in the calculation.

In an actual AFM, only part of the information about tip motion can be acquired, because the real data acquisition process is limited by the bandwidth and precision. The incomplete information will lead to the distortion of the reconstruction. The tip–sample impact forces computed through Eq. (20) are shown in Fig. 4, and the theoretical tip–sample impact force obtained by directed solving the ordinary differential Eqs. (9) is indicated by solid line. The more harmonic components were included in the computation, the more accurate tip–sample impact force was reconstructed. Only the tapping point (peak in time domain) can be roughly calculated by taking one or a few harmonic components into Eq. (20). The numerical results show that the shape of computed tip–sample impact force was close enough to the theoretical one

when we took more then 30 harmonics into computation, which requires the data acquisition speed is above 60 times faster than the tip's free oscillating frequency.

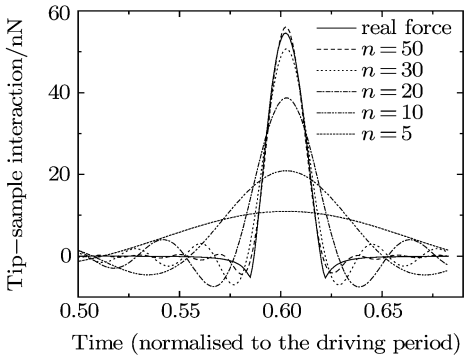


Fig. 4. The tip–sample impact force in time domain computed from tip motion through Eq. (20).

Each time the tip moves toward and then away from the surface, its force varies with distance. This is known as force–distance curve. The force–distance curve is the basis for quantitative material property mapping. The time-vary tip–sample impact force can be converted to a force–distance curve by plotting force versus cantilever flexural bending. These force–distance curves are then analysed to obtain material properties such as stiffness and surface energy. The computed force–distance curves are shown in Fig. 5. The theoretical force–distance curve is indicated by solid line. The stiffness of the sample surface can be computed by the slope of the curve in repulsive force domain, and the surface energy is directly related to the shape of curve in attractive force domain. We can find from the figure that the curves in repulsive force domain are closer to the theoretical force–distance curve than in attractive force domain. Thus the stiffness information of the surface is easier to reconstruct and has a higher precision. Numerical results show that the error of the computed stiffness, based on the values of the first 20 harmonics, from the real surface stiffness is less than 10%.

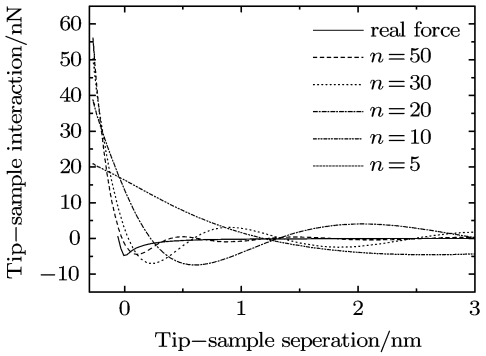


Fig. 5. The computed force–distance curves.

4. Conclusions

In summary, we have shown theoretically that the relationship between the tip motion and tip–sample impact force can be simply expressed as two algebraic formulas. The time-varying tip–sample impact force can be reconstructed by recording and analysing the tip motion. This allows us to make the reconstruction of characteristics of the tip–sample force, such as contact time and maximum contact force. It can also explain the ability of AFM in higher harmonics imaging in mapping stiffness and surface energy variations. Numerical results show that the maximum error of the surface stiffness reconstruction is less than 10%, if the first 20 frequency components are included in the calculation. The present theoretical analysis and the numerical simulation results pave the way to develop a nanometer resolution force spectroscopy for quantitative measurement of the surface mechanical properties.

References

[1] Binnig G, Quate C F and Gerber C 1986 *Phys. Rev. Lett.* **56** 930

[2] García R and Perez R 2002 *Surf. Sci. Rep.* **47** 197

[3] Ou G P, Song Z, Wu Y Y, Chen X Q and Zhang F J 2006 *Chin. Phys.* **15** 1296

[4] Zhong Q, Inniss D, Kjoller K and Elings V B 1993 *Surf. Sci.* **290** L688

[5] Han G Q, Zeng Y G, Yu J Z and Cheng B W 2008 *Chin. Phys. Lett.* **25** 242

[6] Anselmetti D, Luthi R, Meyer E, Richmond T, Dreier M, Frommer J E and Guntherodt H J 2004 *Nanotechnology* **5** 87

[7] Bustamante C and Keller D 1995 *Phys. Today* **48** 33.

[8] Bar G, Thomann Y and Whangbo M H 1998 *Langmuir* **14** 1219

[9] Noy A, Sanders C H, Vezenov D V, Wong S S and Lieber C M 1998 *Langmuir* **14** 1508

[10] Marcus M S, Carpick R W, Sasaki D and Eriksson M A 2002 *Phys. Rev. Lett.* **88** 226103

[11] Cleveland J P, Anczykowski B, Schmid A E and Elings V B 1998 *Appl. Phys. Lett.* **72** 2613

[12] Tamayo J and García R 1997 *Appl. Phys. Lett.* **71** 2394
[13] Tamayo J and García R 1998 *Appl. Phys. Lett.* **73** 2926
[14] Behren O P, Odoni L, Loubet J L and Burnham N A 1999 *Appl. Phys. Lett.* **75** 2551
[15] Patil S, Martinez N F, Lozano J R and García R 2007 *J. Mol. Recognit.* **20** 516
[16] Martinez N F, Lozano J R, Herruzo R T, García F, Richter C, Sulzbach T and García R 2008 *Nanotechnology* **19** 384011
[17] Rodriguez T R and García R 2004 *Appl. Phys. Lett.* **84** 449
[18] Proksch R 2006 *Appl. Phys. Lett.* **89** 113121
[19] Martinez N F, Patil S, Lozano J R and García R 2006 *Appl. Phys. Lett.* **89** 153115
[20] Platz D, Tholen E A, Pensen D and Haviland D B 2008 *Appl. Phys. Lett.* **92** 153106
[21] Stark R W, Naujoks N and Stemmer A 2007 *Nanotechnology* **18** 065502
[22] Stark M, Stark R W, Heckl W M and Guckenberger R 2002 *Proc. Natl. Acad. Sci. USA* **99** 8473
[23] Stark R W and Heckl W M 2003 *Rev. Sci. Instrum.* **74** 5111
[24] Stark R W and Heckl W M 2000 *Surf. Sci.* **457** 219
[25] Legleiter J, Park M, Cusik B and Kowalewski T 2006 *Proc. Natl. Acad. Sci. USA* **103** 4813
[26] Rabe U, Janser K and Arnold W 1996 *Rev. Sci. Instrum.* **67** 3281
[27] Cappella B and Dietler G 1999 *Surf. Sci. Rep.* **34** 1
[28] Fan K Q, Jia J Y, Liu X Y and Zhu Y M 2007 *Acta Phys. Sin.* **56** 6345 (in Chinese)
[29] Derjauin B V, Müller V M and Toporov Y P 1975 *J. Colloid Interface Sci.* **53** 314
[30] García R, Gomez C J, Martinez N F, Patil S, Dietz C and Magerle R 2006 *Phys. Rev. Lett.* **97** 016103
[31] Bausch A R, Ziemann F, Boulbitch A A, Jacobson K and Sackmann E 1998 *Biophys. J.* **75** 2038
[32] Tamayo J and García R 1996 *Langmuir* **12** 4430